Biological Sciences

A bacterial effector protein prevents MAPK-mediated phosphorylation of SGT1 to suppress plant immunity

Gang Yu[1], Liu Xian[1,2], Hao Xue[1,2], Wenjia Yu[1,2], Jose Rufian[1], Yuying Sang[1], Rafael Morcillo[1], Yaru Wang[1,2], and Alberto P. Macho[1,*].

[1]Shanghai Center for Plant Stress Biology, CAS Center for Excellence in Molecular Plant Sciences; Shanghai Institutes of Biological Sciences, Chinese Academy of Sciences, Shanghai 201602, China.

[2]University of Chinese Academy of Sciences, Beijing, China.

* Corresponding author: Alberto P. Macho, alberto.macho@sibs.ac.cn

Keywords: NLR; SGT1; MAPK; ETI; effector; immunity; phosphorylation; virulence; Ralstonia.

Abstract

Nucleotide-binding domain and leucine-rich repeat-containing (NLR) proteins function as sensors that perceive pathogen molecules and activate immunity. In plants, the accumulation and activation of NLRs is regulated by SUPPRESSOR OF G2 ALLELE OF *skp1* (SGT1). In this work, we found that the plant pathogen *Ralstonia solanacearum* secretes an effector protein, named RipAC, inside plant cells, and it associates with SGT1 to suppress NLR-mediated SGT1-dependent immune responses. RipAC does not affect the accumulation of SGT1, NLRs, or their interaction. However, RipAC inhibits the interaction between SGT1 and MAP kinases, and the phosphorylation of a MAPK target motif in the C-terminal domain of SGT1, which is required for the interaction with NLRs. Such phosphorylation releases the interaction between SGT1 and the NLR RPS2, and contributes to the activation of RPS2-mediated responses. Our results shed light onto the mechanism of activation of NLR-mediated immunity, and suggest a positive feedback loop between MAPK activation and SGT1-dependent NLR activation.

Significance Statement

The activation of immune receptors that perceive pathogen molecules and initiate immune signaling is tightly regulated. In plants and animals, SGT1 is a major regulator of the accumulation and activation of such receptors, although the mechanisms of this regulation are not well understood. In this work, we found that the plant pathogenic bacteria *Ralstonia solanacearum*, causal agent of the bacterial wilt disease, secretes an effector protein inside plant cells that suppresses the phosphorylation-dependent activation of SGT1, which in turn inhibits the activation of SGT1-dependent immune receptors. These findings provide new insights into a general mechanism of regulation of immunity, and uncover a new virulence strategy employed by a bacterial pathogen to contribute to disease development.

50 **Introduction**

51 The activation and suppression of plant immunity are key events that determine the
52 outcome of the interaction between plants and bacterial pathogens. When in close
53 proximity to plant cells, conserved bacterial molecules (termed PAMPs, for
54 pathogen-associated molecular patterns) may be perceived by receptors at the
55 surface of plant cells, eliciting the activation of the plant immune system. This leads to
56 the establishment of PAMP-triggered immunity (PTI; (1)), which restricts bacterial
57 growth and prevents the development of disease. Most bacterial pathogens have
58 acquired the ability to deliver proteins inside plant cells via a type-III secretion system
59 (T3SS); such proteins are thus called type-III effectors (T3Es) (2). Numerous T3Es
60 from adapted bacterial plant pathogens have been reported to suppress PTI (3). This,
61 in addition to other T3E activities (4), enables bacterial pathogens to proliferate and
62 cause disease. Resistant plants have evolved mechanisms to detect such bacterial
63 manipulation through the development of intracellular receptors defined by the
64 presence of nucleotide-binding sites (NBS) and leucine-rich repeat domains (LRRs),
65 thus termed NLRs (5). The detection of T3E activities through NLRs leads to the
66 activation of immune responses, which effectively prevent pathogen proliferation (6).
67 The outcome of these responses is named effector-triggered immunity (ETI), and, in
68 certain cases, may cause a hypersensitive response (HR) that involves the collapse
69 of plant cells. In an evolutionary response to this phenomenon, T3E activities have
70 evolved to suppress ETI (7), which in turn exposes bacterial pathogens to further
71 events of effector recognition. For these reasons, the interaction between plants and

microbial pathogens is often considered an evolutionary ‘arms race’, where the specific combination of virulence activities and immune receptors in a certain pathogen-plant pair ultimately defines the outcome of the interaction (7). Although the suppression of PTI by T3Es has been widely documented (3), reports about T3Es that suppress ETI, and their biochemical characterization, remain scarce.

Interestingly, PTI and ETI signaling often involve shared regulators (8), such as mitogen-activated protein kinases (MAPK). The activation of MAPKs is one of the earliest signaling events upon perception of both PAMPs and effectors (9), and is essential for the activation of immune responses. Although sustained MAPK activation has been reported to be critical for the robust development of ETI (10), the signaling events and phosphorylation substrates that link early MAPK activation upon pathogen recognition and downstream MAPK activation as a consequence of NLR activation remain unknown.

The study of microbial effectors has become a very prolific approach to discover and characterize components of the plant immune system and other cellular functions that play important roles in plant-microbe interactions (11). In this regard, T3E repertoires constitute a powerful tool for researchers to understand plant-bacteria interactions. The *Ralstonia solanacearum* species complex (RSSC) groups numerous bacterial strains able to cause disease in more than 250 plant species, including important crops, such as tomato, potato, and pepper, among others (12, 13). *R. solanacearum*

invades the roots of host plants, reaching the vascular system and colonizing xylem vessels in the whole plant, eventually causing their blockage and subsequent plant wilting (14, 15). It has been speculated that the versatility and wide host range of *R. solanacearum* is associated to its relatively large T3E repertoire in comparison with other bacterial plant pathogens; the reference GMI1000 strain serves as an example, being able to secrete more than 70 T3Es (16). Among these T3Es, RipAC (also called PopC; (16, 17) is conserved in most *R. solanacearum* sequenced to date, and is therefore considered a core T3E in the RSSC (Figures S1A and S1B) (16). Domain prediction for the RipAC amino acid sequence reveals the presence of an LRR C-terminal domain and no other predicted enzymatic domain (Figure S1C). Interestingly, it has been shown that RipAC from different *R. solanacearum* strains is promptly expressed upon bacterial inoculation in different host plants (18, 19) suggesting a role in the establishment of the interaction at early stages of the infection process.

Results

RipAC contributes to *R. solanacearum* infection

It is well established that T3Es collectively play an essential role in the development of disease caused by most bacterial plant pathogens, including *R. solanacearum* (20). However, the contribution of individual T3Es to the natural infection process is often difficult to determine, due to functional redundancy among them. To study the contribution of RipAC to *R. solanacearum* infection, we generated a *ΔripAC* mutant strain using the reference phylotype I GMI1000 strain as background (Figure S1D), and confirmed that the growth of this strain in rich laboratory medium is indistinguishable from the wild-type (WT) strain (Figures S1D-1G). We then performed soil-drenching inoculation of Arabidopsis Col-0 WT plants with both WT and *ΔripAC* strains, and monitored the development of wilting symptoms associated to disease. Compared with plants inoculated with WT GMI1000, plants inoculated with the *ΔripAC* mutant displayed attenuated disease symptoms (Figure 1A). This attenuation was complemented by the expression of *ripAC*, driven by its native promoter, in the *ΔripAC* mutant background (Figures 1A and S1E-1G), confirming that virulence attenuation was indeed caused by the lack of the *ripAC* gene. It is noteworthy that, given the intrinsic complexity and biological variability of the soil-drenching inoculation assay, we did not detect a significant attenuation every time we performed this experiment (Figure S2A), suggesting that the attenuation caused by the absence of RipAC is near the limit of detection of this assay.

Tomato is a natural host for several *R. solanacearum* strains (21). To study the contribution of RipAC to *R. solanacearum* virulence during tomato infection, we performed soil-drenching inoculation to compare GMI1000 with the *ΔripAC* strain. As observed in Arabidopsis, tomato plants inoculated with the *ΔripAC* strain showed delayed and/or reduced symptom development in most experiments (Figures 1B and S2B). This attenuation was complemented by the expression of *ripAC* in the mutant background (Figures 1B).

In order to increase the accuracy of our virulence assays and to determine whether the reduced disease symptoms correlate with reduced bacterial multiplication inside host plants, we set up an assay to quantify bacterial numbers in the xylem sap of tomato plants upon injection of the bacterial inoculum in the stem. Compared to plants inoculated with WT GMI1000, plants inoculated with the *ΔripAC* strain showed reduced bacterial numbers, and this was complemented by the expression of *ripAC* in the mutant background (Figure 1C). Altogether, these results suggest that, despite the large effector repertoire of *R. solanacearum* GMI1000, RipAC plays a significant role during the infection process in different host plants.

To complement our genetic analysis of the importance of RipAC in promoting susceptibility to *R. solanacearum*, we generated stable Arabidopsis transgenic lines expressing RipAC from a 35S constitutive promoter (Figures S3A and S3B).

Interestingly, independent transgenic lines expressing RipAC showed enhanced disease symptoms upon soil-drenching inoculation with *R. solanacearum* (Figures 1D and S3C), indicating that RipAC promotes susceptibility to *R. solanacearum* from within plant cells.

RipAC suppresses plant immunity

Plant immunity can be activated by the detection of diverse invasion patterns, either conserved elicitor molecules or strain-specific effector proteins injected inside plant cells (22). To determine whether RipAC has the potential to suppress plant immunity, we performed transient expression of RipAC (fused to a C-terminal GFP tag) in *Nicotiana benthamiana*, and monitored immune responses upon treatment with different invasion patterns. We first tested whether RipAC is able to suppress the fast burst of reactive oxygen species (ROS) triggered by bacterial PAMPs, and found that RipAC expression almost completely blocked the early production of ROS upon treatment with the elicitors flg22^{Pto} (from *Pseudomonas syringae*; Figures 2A and 2B) or csp22^{Rsol} (from *R. solanacearum*; Figures 2C and 2D). We then monitored the induction of cell death associated to the hypersensitive response (HR) developed as part of an ETI response, such as that triggered by overexpression of the NLR-encoding gene *RPS2* (23), the expression of the oomycete effector Avr3a together with the cognate NLR R3a (24), and that triggered by inoculation with *P. syringae pv tomato* DC3000 (*Pto* DC3000) (25). RipAC suppressed the HR triggered by RPS2 and Avr3a/R3a, while it attenuated and delayed HR development in

176 response to *Pto* DC3000 (Figure 2E), showing the potential of RipAC to suppress ETI.
177 Interestingly, RipAC was not able to suppress the cell death triggered by other
178 elicitors, such as Bax (26) and the oomycete elicitor INF1 (27) (Figure 2F), suggesting
179 that RipAC is not a general suppressor of cell death.
180
181 The activation of NLRs is known to trigger the activation of mitogen-activated protein
182 kinases (MAPKs; (10, 28). Consistently, transient overexpression of RPS2 in *N.*
183 *benthamiana* leads to an activation of MAPKs that precedes the onset of macroscopic
184 cell death (Figures 2G and 2H). In our transient expression assays, RipAC
185 significantly suppressed the activation of MAPKs triggered by overexpression of
186 RPS2 or by the expression of Avr3a/R3a (Figures 2I, 2J and 2K), supporting the
187 notion that RipAC suppresses early steps in ETI activation rather than downstream
188 responses that lead to cell death.
189
190 **RipAC interacts with SGT1 from different plant species**
191 To obtain a deeper insight into the mode of action of RipAC, we first investigated the
192 subcellular localization of RipAC inside plant cells. Upon transient expression in *N.*
193 *benthamiana*, RipAC-GFP showed a sharp signal at the cell periphery of leaf
194 epidermal cells (Figure S4A). Upon fractionation of protein extracts from *N.*
195 *benthamiana* expressing RipAC, we detected abundant RipAC in both microsomal
196 and cytosolic fractions (Figure S4B). We then sought to identify plant proteins that
197 physically associate with RipAC in plant cells. To this end, we performed

198 immunoprecipitation (IP) of RipAC-GFP using GFP-trap agarose beads, and analyzed
199 its interacting proteins using liquid chromatography coupled to tandem
200 mass-spectrometry (LC-MS/MS). Together with RipAC-GFP immunoprecipitates, we
201 identified peptides of NbSGT1 (Figure 3A), homolog of the Arabidopsis
202 SUPPRESSOR OF G2 ALLELE OF *skp1* (SGT1), a protein required for the induction
203 of disease resistance mediated by most NLRs (29, 30). The localization of both
204 isoforms of SGT1 in Arabidopsis (AtSGT1a and AtSGT1b) has been reported to be
205 nucleocytoplasmic (31). When we expressed SGT1 (NbSGT1, AtSGT1a, or AtSGT1b)
206 fused to a C-terminal RFP tag, we also detected an apparently cytoplasmic
207 localization, with occasional nuclear localization, although we also detected
208 co-localization with the plasma membrane marker CBL-GFP ((32); Figures S4C and
209 S4D). Interestingly, we detected co-localization between RipAC-GFP and
210 NbSGT1-RFP, AtSGT1a-RFP, or AtSGT1b-RFP (Figure 3B), and these results
211 suggest that RipAC does not affect SGT1 subcellular localization. To confirm the
212 physical interaction between RipAC and SGT1 from different plant species, we
213 co-expressed RipAC-GFP with either NbSGT1, AtSGT1a, AtSGT1b or the tomato
214 ortholog of SGT1b (SlSGT1b). Targeted IP of RipAC-GFP showed CoIP of all
215 different SGT1 orthologs (Figure 3C). To determine if the interaction between RipAC
216 and SGT1 is direct, we performed split-luciferase complementation (Split-LUC)
217 assays in plant cells. In these assays, each protein is fused to a half-luciferase
218 molecule, either N-terminal half of LUC (nLUC) or C-terminal half of LUC (cLUC), and
219 a functional luciferase molecule gets reconstituted if these proteins interact directly

220 (33). The results showed luciferase signal upon expression of RipAC with AtSGT1a,
221 AtSGT1b and NbSGT1 (Figure 3D), suggesting that the interaction between these
222 proteins is direct. We also performed similar split-YFP assays, showing reconstitution
223 of YFP signal at the cell periphery upon expression of RipAC and AtSGT1a, AtSGT1b
224 or NbSGT1 tagged with one of the portions of a split-YFP molecule, indicating a direct
225 interaction of these proteins at the cell periphery (Figure 3E). Altogether, these results
226 indicate that RipAC physically associates with SGT1 from different species inside
227 plant cells.
228
229 SGT1 is conserved in eukaryotes, and has three defined domains: an N-terminal
230 tetratricopeptide repeat (TPR) domain, a CHORD-SGT1 (CS) domain, and a
231 C-terminal SGT1-specific (SGS) domain (34). In order to determine which NbSGT1
232 domain is required for RipAC interaction, we expressed different combinations of
233 these domains (Figure 3F) bound to a FLAG tag, and tested their interaction with
234 immunoprecipitated RipAC-GFP. Although we were unable to express the SGS
235 domain alone, we found an interaction between RipAC and a truncated SGT1 protein
236 containing the CS+SGS domain (Figure 3F). The CS domain alone did not interact
237 with RipAC, suggesting that RipAC associates with the SGS domain, although it
238 cannot be ruled out that RipAC requires both CS+SGS domains to associate with
239 SGT1. Interestingly, the SGS domain is required for all the known SGT1b functions in
240 immunity (31, 34).
241

242 **RipAC inhibits SGT1 interaction with RAR1, but not with the NLR RPS2**

243 In plants, SGT1 associates, though its CS domain, with REQUIRED FOR *Mla12*
244 RESISTANCE (RAR1) and HEAT-SHOCK PROTEIN 90Kda (HSP90) (29, 35, 36),
245 forming a chaperone complex that plays a key role in the accumulation and activation
246 of several NLRs (34). Since RipAC associates with SGT1, we tested whether it also
247 physically interacts with RAR1 and HSP90 in plant cells. Using Split-LUC assays, we
248 found that RipAC interacts with AtRAR1 and with the AtHSP90.2 isoform, but not with
249 AtHSP90.1 (Figure 4A). Given that RipAC interacts directly with all three components
250 of this chaperone complex, we considered the possibility that it may disrupt the
251 formation of the complex. To test this possibility, we performed Split-LUC assays and
252 measure the production of bioluminescence, which provides a quantitative
253 assessment of protein-protein interactions. In this assay, we observed that the
254 expression of RipAC, but not the CBL-GFP control, inhibited significantly the
255 interaction between RAR1 and SGT1a (Figure 4B) and SGT1b (Figure 4C), while it
256 did not seem to affect the accumulation of these proteins (Figure 4D). Such inhibition
257 was also observed in a CoIP assay between AtSGT1a/b fused to a FLAG tag and
258 AtRAR1 fused to a cLUC tag (Figure 4E), indicating that the presence of RipAC
259 disrupts the association between SGT1 and RAR1, most likely as a consequence of
260 its physical interaction with both proteins.

261

262 SGT1 physically associates with several NLRs (37-39); here we found that AtSGT1b
263 also interacts with RPS2 (Figure 4F). To determine whether RipAC interferes with the

interaction between SGT1 and NLRs, we performed Split-LUC assays between AtSGT1b and RPS2 in the presence of RipAC. Interestingly, RipAC did not affect RPS2 accumulation or the interaction between AtSGT1b and RPS2 (Figures 4F and 4G), indicating that RipAC does not generally disrupt all the interactions in the SGT1 complex.

RipAC inhibits SGT1-mediated immune responses in *N. benthamiana* and Arabidopsis

SGT1 is an essential component of the plant immune system, due to its role as a regulator of the stability and activation of most NLRs, and it is required for the establishment of ETI (34). Since we have shown that RipAC suppresses NLR-mediated responses associated to both bacterial and oomycete pathogens (Figures 2E and 2I-2K), we wondered whether RipAC could suppress other SGT1-mediated signaling events in plant cells. Expression of a constitutively active form of the Arabidopsis MAPK Kinase 7 (AtMKK7DD) in *N. benthamiana* leads to cell death in an SGT1-dependent manner (40). The simultaneous expression of RipAC abolished the macroscopic cell death triggered by overexpression of AtMKK7DD in *N. benthamiana* (Figures 5A and 5B). We also observed that AtMKK7DD overexpression in *N. benthamiana* led to the activation of the MAPKs SIPK and WIPK, and, similarly, RipAC inhibited such MAPK activation (Figures 5B and 5C). These results indicate that RipAC is able to suppress ETI-associated SGT1-dependent responses from different origins in *N. benthamiana*.

To determine whether RipAC inhibits the final outcome of ETI (i.e. restriction of bacterial proliferation), we inoculated RipAC-expressing Arabidopsis transgenic lines (Figures S3A and S3B) by infiltrating leaves with a suspension of *Pto* DC3000 expressing different T3Es that activate NLR-dependent immunity, namely AvrRpm1 (41), AvrRpt2 (42), or AvrRps4 (43). Such strains, compared to *Pto* DC3000 expressing an empty vector (EV) (Figure 5D), show deficient replication in Arabidopsis, due to immune responses triggered by these T3Es (Figures 5E-5G). However, different transgenic lines expressing RipAC showed enhanced susceptibility to these strains (Figures 5E-5G), indicating that RipAC is able to effectively suppress NLR-mediated immunity in Arabidopsis.

SGT1 is not required for PTI responses in *N. benthamiana* and Arabidopsis

Since RipAC suppresses ROS burst triggered by bacterial elicitors and seems to disrupt SGT1-dependent immune responses, we considered the possibility that SGT1 may also be required for early PTI signaling. To explore this possibility, we first used virus-induced gene silencing (VIGS) to silence *SGT1* expression in *N. benthamiana*. Although VIGS abolished *NbSGT1* expression, this did not affect the ROS burst triggered by flg22^{Pto} or csp22^{Rsol}, suggesting that NbSGT1 is not required for early PTI signaling in *N. benthamiana* (Figures S5A-S5D). In Arabidopsis, a double mutation in *AtSGT1a* and *AtSGT1b* is not viable, suggesting that both genes have redundant functions in plant development besides their contribution to immunity (44). However,

we observed that the knockout mutants *sgt1a-1* (Ws-0 background) and *sgt1b-3* (La-*er* background) show different developmental phenotypes compared to their respective WT controls (Figure S5E). Moreover, when treated with the elicitor peptide elf18 from either *P. syringae* or *R. solanacearum*, the *sgt1a-1* mutant showed attenuated ROS burst, while the *sgt1b-3* mutant showed enhanced ROS burst, compared to their respective WT controls (Figures S5F-S5I). Despite these differences, neither of these mutants showed altered MAPK activation triggered by elf18 (Figures S5J and S5K), nor altered susceptibility upon inoculation with a *Pto* T3SS- mutant (Figures S5L and S5M). This suggests that, although AtSGT1a and AtSGT1b may have a different contribution to early PTI signaling, they are not collectively required for the establishment of PTI. To overcome the observed partial redundancy of AtSGT1a and AtSGT1b, we performed VIGS of *AtSGT1a* in *sgt1b-3* mutant plants (Figure S5N). *AtSGT1a* VIGS reduced the accumulation of AtSGT1a, as revealed by western blot analysis (Figure S5O), sufficient to render silenced plants more susceptible to *Pto* expressing AvrRpt2 (Figure S5R), suggesting that these plants have impaired SGT1 functions in the establishment of ETI. On the contrary, the silenced plants were not more susceptible to a *Pto* T3SS- mutant (or to WT *Pto* DC3000) (Figures S5P and S5Q), suggesting that abolishing SGT1 function in Arabidopsis does not have a major impact in the establishment of PTI. Altogether, we concluded that the targeting of SGT1 does not account for the RipAC-mediated suppression of PTI, and focused on the study of a potential inhibition of SGT1 function by RipAC.

330

331 **MAPK-mediated phosphorylation is important for SGT1 function in the**
332 **activation of ETI**

333 Since post-translational modifications (PTMs) have been shown to impact SGT1
334 function (45-47), we sought to determine whether RipAC causes any alteration of
335 SGT1 PTMs in plant cells. To this end, we co-expressed NbSGT1 fused to a FLAG
336 tag together with RipAC (or a GFP control) in *N. benthamiana* leaves, and then
337 performed IP using an anti-FLAG resin followed by LC-MS/MS. Among the IPed
338 SGT1 peptides, we detected two peptides, located in the SGS domain, containing
339 phosphorylated serine residues (S282 and S358) (Figure S6). Interestingly, a
340 phosphorylable residue is conserved in these positions among plants from different
341 species (Figures S7A), and S358 is embedded in a canonical MAPK-mediated
342 phosphorylation motif conserved across the plant kingdom (Figure S7B). Interestingly,
343 AtSGT1b has been shown to interact with MAPK4 (48), and SGT1 from tobacco
344 (NtSGT1) S358, equivalent to T346 in AtSGT1b, has been shown to be
345 phosphorylated by NtSIPK (45). By performing targeted CoIP, we found that both
346 AtSGT1a and AtSGT1b associate with AtMAPK4 and AtMAPK6, but not with
347 AtMAPK3, which showed very low accumulation in this assay (Figure 6A). The
348 association of both AtSGT1a and AtSGT1b with AtMAPK3 and AtMAPK4, but not with
349 AtMAPK6, was also shown by Split-LUC (Figure S8). To determine whether
350 MAPK-mediated SGT1 phosphorylation is enhanced upon activation of ETI, we raised
351 an antibody against the potential MAPK phosphorylated peptide, conserved in both

352 AtSGT1a and AtSGT1b, containing phosphorylated T346 (ESpTPPDGME), which
353 specifically detected the phosphorylated peptide *in vitro* and *in planta* (Figures S9A
354 and S9B). Inoculation of Arabidopsis plants with *Pto* expressing AvrRpt2 or AvrRps4,
355 but not with *Pto* DC3000 or *Pto* TTSS-, led to a sustained activation of MAPKs and to
356 enhanced phosphorylation of T346 (Figure S9C). Similarly, dexamethasone-induced
357 expression of AvrRpt2 in Arabidopsis transgenic lines led to MAPK activation and
358 enhanced SGT1 phosphorylation (Figures 6B and 6C). These data indicate that T346
359 phosphorylation occurs concomitantly to the activation of ETI.
360
361 To determine the relevance of the phosphorylation of SGT1 S271/T346 for the
362 activation of ETI, we generated single and double point mutants in these residues in
363 AtSGT1b, substituting them for alanine residues (to abolish phosphorylation) or for
364 aspartate residues (to mimic the negative charge associated to constitutive
365 phosphorylation). Due to the difficulties in genetic analysis of SGT1, we used a
366 transient approach in *N. benthamiana*, co-expressing the AtSGT1b variants together
367 with RPS2. Alanine mutations (S271A/T346A: AtSGT1b AA) did not have a
368 detectable impact on the RPS2-mediated cell death (Figure 6D), likely due to the
369 presence of endogenous NbSGT1. However, tissues expressing both the T346D
370 mutant (2D) or the double S271D/T346D (DD) mutant, but not the single S271D
371 mutant, showed an enhancement of cell death triggered by RPS2 expression,
372 monitored as ion leakage (Figure 6D), which correlated with the appearance of tissue

373 necrosis (Figures 6E and 6F). This suggests that T346 phosphorylation contributes to
374 the robust activation of ETI responses.
375
376 Previous reports have shown that SGT1 phosphorylation seems to enhance SGT1
377 nuclear localization (45, 46). However, neither the SGT1 AA nor DD showed any
378 obvious differential localization compared with WT AtSGT1b in our system (Figure
379 S10A). Given the importance of protein-protein interactions in the SGT1 complex, we
380 hypothesized that phosphorylation in S271/T346 may be important to regulate the
381 interaction of SGT1 with either RAR1 or NLRs. However, neither alanine or aspartate
382 substitutions in these residues had an impact on the interaction between AtSGT1b
383 and RAR1 (Figure 6G). Similarly, the T346A mutation did not affect the interaction
384 between AtSGT1b and RPS2 (Figure 6H); however, surprisingly, the T346D mutation
385 inhibited this interaction (Figure 6H and S10B). This, together with the observation
386 that the T346D mutation causes an enhancement of RPS2-triggered responses,
387 suggests a scenario where phosphorylation contributes to the release of RPS2 from
388 the SGT1 complex to activate immune responses.
389
390 **RipAC interferes with the MAPK-SGT1 interaction to suppress SGT1**
391 **phosphorylation**
392 During our analysis of SGT1 phosphorylation, we observed an apparent reduction in
393 the number of SGT1 phosphorylated peptides in the presence of RipAC (Figure S6A).
394 Since this assay does not allow a comparative quantitative assessment of SGT1

395 phosphorylation, we took advantage of the sensitivity of our anti-pSGT1 antibody to
396 determine the impact of RipAC on the phosphorylation of AtSGT1 T346. Interestingly,
397 Arabidopsis transgenic lines expressing RipAC showed reduced phosphorylation of
398 T346 in endogenous SGT1 in basal growth conditions (Figures 7A and 7B). Such
399 reduction of T346 phosphorylation was also observed when Arabidopsis protoplasts
400 were transfected with RipAC in the presence of AvrRpt2 (Figures 7C and 7D),
401 indicating that RipAC suppresses the phosphorylation of AtSGT1 T346.
402
403 Since we have shown that RipAC inhibits the interaction of SGT1 with RAR1, we
404 considered the possibility that RipAC suppresses SGT1 phosphorylation by interfering
405 with the MAPK-SGT1 interaction. This interference was indeed confirmed by
406 Split-LUC and CoIP assays, which showed that RipAC inhibits the interaction of SGT1
407 with all AtMAPK3, AtMAPK4 and AtMAPK6 (Figures 7E-7G), suggesting that this is
408 the mechanism underlying RipAC suppression of SGT1-dependent ETI responses
409 (Figure S11).
410
411
412 **Discussion**
413 The targeting of ETI regulators by effector proteins represents a powerful strategy for
414 bacterial pathogens to avoid perception by the plant or to mitigate its consequences.
415 The dual character of effectors as triggers and suppressors of immunity drives the
416 specific evolution of effectors and plant resistance proteins, and ultimately defines the

417 outcome of the interaction. Despite the importance of T3Es for the bacterial infection
418 process, single effector knockout mutants often lack virulence phenotypes due to
419 functional redundancy among effectors. This may be particularly important in strains
420 belonging to the *R. solanacearum* species complex, where single strains may secrete
421 more than 70 T3Es (16). Before, a *ΔripAC* mutant strain was reported to show
422 reduced fitness, compared to GMI1000, in eggplant leaves (49). Here we show that
423 an equivalent mutant has impaired virulence in Arabidopsis and tomato, and such
424 attenuation is complemented by the expression of the effector, indicating that RipAC
425 plays a significant role in the *R. solanacearum* infection process.
426
427 In this work, we found that RipAC interacts with SGT1, a major regulator of the activity
428 of NLRs in the activation of ETI (34). SGT1 has been shown to regulate NLR
429 homeostasis, either by contributing to protein stability or by mediating their
430 degradation (44, 50). RipAC was able to interact with a truncated SGT1 containing
431 only the CS+SGS domains, but not with the CS domain alone, suggesting that RipAC
432 interacts with the SGS domain, or that it requires both CS and SGS domains for
433 interaction. The CS domain has been shown to mediate the interaction between
434 SGT1 and its cognate co-chaperones RAR1 and HSP90 (35, 36). Interestingly, RipAC
435 prevents the interaction between SGT1 and RAR1, suggesting that it affects the
436 interaction surface at the CS domain, and it is reasonable to hypothesize that this
437 contributes to its ability to suppress ETI (Figure S11). The SGS domain is essential for
438 SGT1 immune functions and mediates SGT1 interaction with the LRRs of NLRs and

439 the co-chaperone HSC70 (31), although its biochemical function remains unclear. We
440 found that RipAC prevents the interaction between MAPKs and SGT1 in plant cells,
441 leading to a reduced phosphorylation of SGT1 in the SGS domain, suggesting that
442 MAPKs also interact with this domain. MAPKs have been shown to phosphorylate
443 SGT1 from tobacco and maize in *N. benthamiana* (45, 47), contributing to the
444 hypothesis that MAPK-mediated phosphorylation of SGT1 may be important for its
445 function. This notion is also supported by our data, showing that mutations that mimic
446 phosphorylation in the observed SGT1 phosphosites lead to an enhanced activity of
447 the NLR RPS2 (Figure S11). Although, in previous reports, SGT1 phosphorylation
448 seems to enhance SGT1 nuclear localization (45, 46), our phosphorylation-related
449 SGT1 mutants did not show any obvious differential localization compared with WT
450 SGT1. Interestingly, the enhanced RPS2 activity caused by the T346D
451 phospho-mimic mutation correlated with an enhanced dissociation between SGT1
452 (T346D) and RPS2, suggesting that MAPK-mediated phosphorylation of SGT1 may
453 contribute to NLR activation through the modulation of SGT1 interactions with NLRs
454 (Figure S11). Considering that NLR activation leads to enhanced MAPK activation,
455 this regulatory mechanism would represent a positive feedback loop between the
456 activation of NLRs and MAPKs, mediated by the phosphorylation of SGT1 (Figure
457 S11). Intriguingly, although RipAC suppresses SGT1-dependent immune responses,
458 it does not seem to affect the accumulation of SGT1 or NLRs (in our case, RPS2),
459 which resembles the phenotype observed upon overexpression of the
460 SGS-interacting protein HSC70 (31). Altogether, our data suggest that, by associating

with the SGS domain, RipAC compromises SGT1 interaction with MAPKs and the subsequent phosphorylation of specific sites in the SGS domain, compromising the activation of immunity without altering the accumulation of associated proteins (Figure S11). Moreover, SGT1 phosphorylation in the SGS domain does not seem to be required for SGT1 interaction with the other components of the chaperone complex (mediated by the CS domain). Consistently, a mutant including a premature stop codon at P347 in AtSGT1b, disrupting the MAPK phosphorylation motif that includes T346, does not affect the formation of the SGT1/RAR1/HSP90 complex, but abolishes the immune-associated functions of SGT1 (35). Therefore, further work will be required to determine whether the RipAC-mediated inhibition of SGT1-RAR1-HSP90 interactions and MAPK-mediated SGT1 phosphorylation have an additive effect in blocking SGT1 functions.

Although the contribution of SGT1 to the establishment of ETI is well-known, genetic analysis of its contribution to disease resistance is challenging, due to the deleterious effects caused by the abolishment of SGT1 expression (34). However, Arabidopsis transgenic plants expressing RipAC become more susceptible to *R. solanacearum* infection, suggesting the importance of SGT1 function for resistance against *R. solanacearum*, although we should consider that other potential targets of RipAC may also account for the enhanced susceptibility of RipAC-expressing transgenic plants. In this regard, we found that RipAC also suppresses PTI responses in *N. benthamiana*, and this activity does not seem to be ascribed to the targeting of SGT1. This suggests

483 that the RipAC-mediated suppression of PTI is due to the additional targeting of other
484 immune regulators.
485
486 The T3E AvrBsT from *Xanthomonas campestris* also interacts with SGT1 from pepper,
487 and interferes with its phosphorylation by the PIK1 kinase in two serine residues (in
488 the CS domain and variable region) different from the ones identified in our study (46).
489 However, in that case, AvrBsT triggers SGT1-mediated immunity, and the identified
490 SGT1 phosphorylation sites are required for the activation of AvrBsT-triggered HR
491 (46). Similarly, a secreted effector from the fungal pathogen *Ustilago maydis* also
492 interferes with the MAPK-mediated phosphorylation of SGT1 from maize in a
493 monocot-specific phosphorylation site between TPR and CS domains, contributing to
494 the development of disease-associated tumors (47). This demonstrates that
495 pathogens from different kingdoms and with different lifestyles have evolved to target
496 different functions of SGT1 as a key regulator of disease resistance. Considering that
497 SGT1 interacts with and regulates the function of proteins containing LRRs (such as
498 NLRs), it is tantalizing to hypothesize that RipAC may have acquired an LRR domain
499 to associate with SGT1 and disrupt its function. This virulence strategy may be a case
500 of convergent evolution between bacterial pathogens of plants and animals, since
501 *Salmonella typhimurium* similarly delivers an LRR-containing effector, Ssph2, which
502 also interacts with SGT1 in animal and plant cells (51). However, as in the case of
503 AvrBsT, Ssph2 seems to stimulate SGT1-dependent immunity (51). Altogether, this
504 suggests that, although effector proteins from different microbial pathogens associate

with SGT1, some of them are indeed perceived by the plant immune system, potentially as a consequence of the 'guarding' of SGT1 as an important regulator of plant immunity. On the contrary, RipAC seems to manipulate SGT1 for virulence purposes without being detected by the plant immune system, suggesting that these host plants have not yet evolved a perception system for this targeting. Together with other reports, our discovery of the molecular mechanisms underlying the RipAC-mediated suppression of SGT1 function may contribute to the engineering of functional SGT1 complexes that abolish bacterial manipulation or respond to it by activating immunity. Interestingly, *R. solanacearum* injects other T3Es containing LRRs (16). It will be interesting to determine whether other T3Es employ LRR domains to target plant proteins that rely on LRR-mediated interactions for their function.

Materials and methods

All the experimental procedures are detailed in the supporting Materials and Methods section. The biological and chemical resources used in this study are summarized in the Table S1.

Acknowledgements

We thank Nemo Peeters and Anne-Claire Cazale for sharing unpublished biological materials, Yasuhiro Kadota and Ken Shirasu for helpful discussions and sharing biological materials, Suomeng Dong, Jian-Min Zhou, Gitta Coaker, and Laurent Deslandes for sharing biological materials, Rosa Lozano-Duran for critical reading of

528 this manuscript, and Xinyu Jian for technical and administrative assistance during this
529 work. We thank the PSC Cell Biology and Proteomics core facilities for assistance
530 with confocal microscopy and LC-MS/MS analysis, respectively. This work was
531 supported by the Strategic Priority Research Program of the Chinese Academy of
532 Sciences (grant XDB27040204), the National Natural Science Foundation of China
533 (NSFC; grant 31571973), the Chinese 1000 Talents Program, and the Shanghai
534 Center for Plant Stress Biology (Chinese Academy of Sciences). Gang Yu was
535 partially supported by the China Postdoctoral Science Foundation (grant
536 2016M600339). The authors have no conflict of interest to declare.

537

538

References

1. Boller T & Felix G (2009) A renaissance of elicitors: perception of microbe-associated molecular patterns and danger signals by pattern-recognition receptors. *Annual Review of Plant Biology* 60(1):379-406.
2. Galán JE, Lara-Tejero M, Marlovits TC, & Wagner S (2014) Bacterial type III secretion systems: specialized nanomachines for protein delivery into target cells. *Annual Review of Microbiology* 68(1):415-438.
3. Macho AP & Zipfel C (2015) Targeting of plant pattern recognition receptor-triggered immunity by bacterial type-III secretion system effectors. *Current Opinion in Microbiology* 23:14-22.
4. Macho AP (2016) Subversion of plant cellular functions by bacterial type-III effectors: beyond suppression of immunity. *New Phytologist* 210(1):51-57.
5. Cui H, Tsuda K, & Parker JE (2015) Effector-triggered immunity: from pathogen perception to robust defense. *Annual Review of Plant Biology* 66(1):487-511.
6. Chiang Y-H & Coaker G (2015) Effector triggered immunity: NLR immune perception and downstream defense responses. *The Arabidopsis Book*:e0183.
7. Jones JDG & Dangl JL (2006) The plant immune system. *Nature* 444(7117):323-329.
8. Tsuda K & Katagiri F (2010) Comparing signaling mechanisms engaged in pattern-triggered and effector-triggered immunity. *Current Opinion in Plant Biology* 13(4):459-465.
9. Meng X & Zhang S (2013) MAPK cascades in plant disease resistance signaling. *Annual Review of Phytopathology* 51(1):245-266.
10. Tsuda K*, et al.* (2013) Dual regulation of gene expression mediated by extended MAPK activation and salicylic acid contributes to robust innate immunity in *Arabidopsis thaliana*. *PLoS Genetics* 9(12):e1004015.
11. Toruño TY, Stergiopoulos I, & Coaker G (2016) Plant-pathogen effectors: cellular probes interfering with plant defenses in spatial and temporal manners. *Annual Review of Phytopathology* 54(1):419-441.
12. Jiang G*, et al.* (2017) Bacterial wilt in China: history, current status, and future perspectives. *Frontiers in Plant Science* 8(1549).
13. Mansfield J*, et al.* (2012) Top 10 plant pathogenic bacteria in molecular plant pathology. *Molecular Plant Pathology* 13(6):614-629.
14. Digonnet C*, et al.* (2012) Deciphering the route of *Ralstonia solanacearum* colonization in *Arabidopsis thaliana* roots during a compatible interaction: focus at the plant cell wall. *Planta* 236(5):1419-1431.
15. Turner M*, et al.* (2009) Dissection of bacterial wilt on *Medicago truncatula* revealed two type III secretion system effectors acting on root infection process and disease development. *Plant Physiology* 150(4):1713-1722.

16. Peeters N, *et al.* (2013) Repertoire, unified nomenclature and evolution of the Type III effector gene set in the *Ralstonia solanacearum* species complex. *BMC Genomics* 14(1):859.
17. Guéneron M, Timmers ACJ, Boucher C, & Arlat M (2000) Two novel proteins, PopB, which has functional nuclear localization signals, and PopC, which has a large leucine-rich repeat domain, are secreted through the Hrp-secretion apparatus of *Ralstonia solanacearum*. *Molecular Microbiology* 36(2):261-277.
18. Jacobs JM, Babujee L, Meng F, Milling A, & Allen C (2012) The *in planta* transcriptome of *Ralstonia solanacearum* conserved physiological and virulence strategies during bacterial wilt of tomato. *mBio* 3(4):e00114-00112.
19. Puigvert M, *et al.* (2017) Transcriptomes of *Ralstonia solanacearum* during root colonization of *Solanum commersonii*. *Frontiers in Plant Science* 8(370).
20. Deslandes L & Genin S (2014) Opening the *Ralstonia solanacearum* type III effector tool box: insights into host cell subversion mechanisms. *Current Opinion in Plant Biology* 20:110-117.
21. Hayward AC (1991) Biology and epidemiology of bacterial wilt caused by *Pseudomonas Solanacearum*. *Annual Review of Phytopathology* 29(1):65-87.
22. Cook DE, Mesarich CH, & Thomma BPHJ (2015) Understanding plant immunity as a surveillance system to detect invasion. *Annual Review of Phytopathology* 53(1):541-563.
23. Jin H, *et al.* (2002) NPK1, an MEKK1-like mitogen-activated protein kinase kinase kinase, regulates innate immunity and development in plants. *Developmental Cell* 3(2):291-297.
24. Armstrong MR, *et al.* (2005) An ancestral oomycete locus contains late blight avirulence gene *Avr3a*, encoding a protein that is recognized in the host cytoplasm. *Proceedings of the National Academy of Sciences of the United States of America* 102(21):7766-7771.
25. Wei C-F, *et al.* (2007) A *Pseudomonas syringae* pv. *tomato* DC3000 mutant lacking the type III effector HopQ1-1 is able to cause disease in the model plant *Nicotiana benthamiana*. *The Plant Journal* 51(1):32-46.
26. Lacomme C & Santa Cruz S (1999) Bax-induced cell death in tobacco is similar to the hypersensitive response. *Proceedings of the National Academy of Sciences* 96(14):7956-7961.
27. Kamoun S, van West P, Vleeshouwers VGAA, de Groot KE, & Govers F (1998) Resistance of *Nicotiana benthamiana* to *Phytophthora infestans* is mediated by the recognition of the elicitor protein INF1. *The Plant Cell* 10(9):1413-1425.
28. Adachi H, *et al.* (2015) WRKY transcription factors phosphorylated by MAPK regulate a plant immune NADPH oxidase in *Nicotiana benthamiana*. *The Plant Cell* 27(9):2645-2663.
29. Azevedo C, *et al.* (2002) The RAR1 interactor SGT1, an essential component of *R* gene-triggered disease resistance. *Science* 295(5562):2073-2076.
30. Kadota Y, Shirasu K, & Guerois R (2010) NLR sensors meet at the SGT1-HSP90 crossroad. *Trends in Biochemical Sciences* 35(4):199-207.

31. Noël LD, *et al.* (2007) Interaction between SGT1 and cytosolic/nuclear HSC70 chaperones regulates Arabidopsis immune responses. *The Plant Cell* 19(12):4061-4076.
32. Gao Z, Chung E-H, Eitas TK, & Dangl JL (2011) Plant intracellular innate immune receptor Resistance to *Pseudomonas syringae* pv. maculicola 1 (RPM1) is activated at, and functions on, the plasma membrane. *Proceedings of the National Academy of Sciences of the United States of America* 108 (18):7619-7624.
33. Chen H, *et al.* (2008) Firefly luciferase complementation imaging assay for protein-protein interactions in plants. *Plant Physiology* 146(2):368-376.
34. Shirasu K (2009) The HSP90-SGT1 chaperone complex for NLR immune sensors. *Annual Review of Plant Biology* 60(1):139-164.
35. Botër M, *et al.* (2007) Structural and functional analysis of SGT1 reveals that its interaction with HSP90 is required for the accumulation of Rx, an R protein involved in plant immunity. *The Plant Cell* 19(11):3791-3804.
36. Zhang M, Kadota Y, Prodromou C, Shirasu K, & Pearl LH (2010) Structural basis for assembly of Hsp90-Sgt1-CHORD protein complexes: implications for chaperoning of NLR innate immunity receptors. *Molecular Cell* 39(2):269-281.
37. Bieri S, *et al.* (2004) RAR1 positively controls steady state levels of barley MLA resistance proteins and enables sufficient MLA6 accumulation for effective resistance. *The Plant Cell* 16(12):3480-3495.
38. Kud J, *et al.* (2013) SGT1 interacts with the Prf resistance protein and is required for Prf accumulation and Prf-mediated defense signaling. *Biochemical and Biophysical Research Communications* 431(3):501-505.
39. Leister RT, *et al.* (2005) Molecular genetic evidence for the role of *SGT1* in the intramolecular complementation of Bs2 protein activity in *Nicotiana benthamiana*. *The Plant Cell* 17(4):1268-1278.
40. Popescu SC, *et al.* (2009) MAPK target networks in *Arabidopsis thaliana* revealed using functional protein microarrays. *Genes & Development* 23(1):80-92.
41. Grant M, *et al.* (1995) Structure of the Arabidopsis RPM1 gene enabling dual specificity disease resistance. *Science* 269(5225):843-846.
42. Bent A, *et al.* (1994) RPS2 of *Arabidopsis thaliana*: a leucine-rich repeat class of plant disease resistance genes. *Science* 265(5180):1856-1860.
43. Gassmann W, Hinsch ME, & Staskawicz BJ (1999) The Arabidopsis RPS4 bacterial-resistance gene is a member of the TIR-NBS-LRR family of disease-resistance genes. *The Plant Journal* 20(3):265-277.
44. Azevedo C, *et al.* (2006) Role of SGT1 in resistance protein accumulation in plant immunity. *The EMBO Journal* 25(9):2007-2016.
45. Hoser R, *et al.* (2013) Nucleocytoplasmic partitioning of tobacco N receptor is modulated by SGT1. *New Phytologist* 200(1):158-171.
46. Kim NH, Kim DS, Chung EH, & Hwang BK (2014) Pepper suppressor of the G2 allele of *skp1* interacts with the receptor-like cytoplasmic kinase1 and type

III effector AvrBsT and promotes the hypersensitive cell death response in a phosphorylation-dependent manner. *Plant Physiology* 165(1):76-91.

47. Redkar A*, et al.* (2015) A secreted effector protein of *Ustilago maydis* guides maize leaf cells to form tumors. *The Plant Cell* 27(4):1332-1351.

48. Cui H*, et al.* (2010) *Pseudomonas syringae* effector protein AvrB perturbs Arabidopsis hormone signaling by activating MAP Kinase 4. *Cell Host & Microbe* 7(2):164-175.

49. Macho AP, Guidot A, Barberis P, Beuzón CR, & Genin S (2010) A competitive index assay identifies several *Ralstonia solanacearum* type III effector mutant strains with reduced fitness in host plants. *Molecular plant-microbe interactions : MPMI* 23(9):1197-1205.

50. Holt BF, Belkhadir Y, & Dangl JL (2005) Antagonistic control of disease resistance protein stability in the plant immune system. *Science* 309(5736):929-932.

51. Bhavsar AP*, et al.* (2013) The Salmonella type III effector SspH2 specifically exploits the NLR co-chaperone activity of SGT1 to subvert immunity. *PLoS Pathogens* 9(7):e1003518.

Figure legends

Figure 1. RipAC contributes to *Ralstonia solanacearum* virulence in Arabidopsis and tomato. (A, B) Soil-drenching inoculation assays in Arabidopsis (A) and tomato (B) were performed with GMI1000 WT, D*ripAC* mutant, and RipAC complementation (*ripAC*$^+$) strains. n=15 plants per genotype (for Arabidopsis) or n=12 plants per genotype (for tomato). The results are represented as disease progression, showing the average wilting symptoms in a scale from 0 to 4 (mean ± SEM). (C) Growth of *R. solanacearum* GMI1000 WT, D*ripAC* mutant, and RipAC complementation (*ripAC*$^+$) strains in tomato plants. 5 µL of bacterial inoculum (10^6 cfu mL^{-1}) were injected into the stem of 4-week-old tomato plants and xylem sap was taken from each infected plants for bacterial titer calculation 3 days post-inoculation

699 (dpi) (mean ± SEM, n=6, ** p<0.01, *t*-test). (D) Soil-drenching inoculation assays in
700 Col-0 WT and RipAC-expressing Arabidopsis lines (AC #3, AC #31, two independent
701 lines) with GMI1000 WT strain. Results are represented as in A and B.
702 See also Figures S1, S2 and S3.
703
704 **Figure 2. RipAC inhibits plant immune responses in *Nicotiana benthamiana***
705 **leaves.**
706 (A-D) RipAC suppresses ROS burst triggered by flg22^{Pto} (A and B) and csp22^{Rsol} (C
707 and D). RipAC-GFP or GFP (as control) were transiently expressed in 5-week-old for
708 flg22) or 6-week-old (for csp22) *N. benthamiana* leaves and ROS burst was analyzed
709 after treatment with the respective elicitors (50 nM) using a luminol-based assay
710 (mean ± SEM, n=24). These experiments were performed at least 3 times with similar
711 results. (E) RipAC suppresses RPS2-, Avr3a/R3a-, *Pto* DC3000-associated cell death.
712 (F) RipAC does not suppress BAX- or INF1-induced cell death. Photographs were
713 taken 5 days after the expression of the cell death inducer. The numbers beside the
714 photographs indicate the ratios of infiltration showing the presented result among the
715 total number of infiltrations. (G and H) The induction of cell death triggered by
716 overexpression of RPS2 (G) correlates with the activation of the MAPKs NbSIPK and
717 NbWIPK (H) in a time course assay different hours post-inoculation (hpi) with
718 Agrobacterium leading to the expression of RPS2. In (G), RPS2-triggered cell death
719 was monitored by visible light and UV light. In (H), phosphorylation of NbSIPK and
720 NbWIPK was detected using anti-pMAPK antibody. (I and J) RipAC suppresses

721 MAPK activation triggered by the overexpression of RPS2 (I) or Avr3a/R3a (J), 24 hpi
722 with Agrobacterium leading to the expression of the cell death inducers. (K)
723 Quantification of relative pMAPK in (I) and (J). The quantification of the pMAPK band
724 in RipAC expression spots is represented relative to the intensity in the GFP control in
725 each assay (mean ± SEM of 4 independent biological replicates).
726
727 **Figure 3. RipAC associates with SGT1 in plant cells.**
728 (A) RipAC-GFP or free GFP were transiently expressed in *N. benthamiana* leaves.
729 The figure shows the unique NbSGT1 peptides identified exclusively in RipAC-GFP
730 sample upon GFP immunoprecipitation followed by IP-MS/MS analysis. (B)
731 RipAC-GFP co-localizes with SGT1-RFP in plant cells. RipAC-GFP was transiently
732 co-expressed with SGT1-RFP (AtSGT1a, AtSGT1b, or NbSGT1), and the GFP
733 fluorescence signal was observed 48 hpi using confocal microscopy. The images
734 show the fluorescence from GFP, RFP channel, and the merged fluorescence from
735 both channels. The corresponding fluorescence intensity profiles (GFP, green; RFP,
736 red) across the green lines are shown. Scale bar=50 μm. (C) CoIP to determine
737 interactions between RipAC and SGT1s. The signal in the interaction between RipAC
738 and AtSGT1a was weak and is shown with longer exposure. (D) Split-LUC assay, and
739 (E) split-YFP complementation assay, to determine direct interaction between RipAC
740 and SGT1 in plant cells. In (E), the self-association of aquaporin AtPIP2A was used
741 as a positive interaction control, while the RipAC-AtPIP2A combination was used as a
742 negative control. Scale bar=50 μm. (F) CoIP to determine interactions between RipAC

743 and different truncated versions of NbSGT1. The diagram summarizes the different
744 domains of SGT1: TPR, N-terminal tetratricopeptide repeat (TPR) domain; CS,
745 CHORD-SGT1 domain; SGS, C-terminal SGT1-specific domain; VR, variable region.
746 In C-F, each combination of proteins shown was transiently expressed in *N.*
747 *benthamiana* and samples were taken 2 dpi. Experiments shown in (B-E), were
748 performed 3 times with similar results. The experiment shown in (F) was performed
749 twice.
750 See also Figure S4.
751
752 **Figure 4. RipAC interferes with the SGT1-RAR1 complex.**
753 (A) RipAC associates with SGT1, RAR1, and HSP90. Split-LUC assay was performed
754 as in the Fig. 3F. (B) and (C) Competitive Split-LUC assays showing that RipAC
755 interferes with SGT1a/b-RAR1 complex formation. The FLS2-SGT1 combination was
756 used as negative interaction control. In quantitative assays, the graphs show the
757 mean value ± SEM (n=12, ** $p<0.01$, *t*-test). (D) Protein accumulation from (B) and
758 (C). (E) Competitive CoIP showing that RipAC interferes with SGT1a/b-RAR1
759 complex formation. Anti-FLAG beads were used to IP AtSGT1a and AtSGT1b. (F)
760 Competitive Split-LUC showing that RipAC does not interfere with RPS2-SGT1b
761 association. (G) Western blot shows the protein accumulation in (F). The
762 RPS2-PIP2A combination was used as negative control. In all the competitive
763 interaction assays, in addition to the interaction pair, RipAC or CBL-GFP (as negative
764 control) were expressed to determine interference. In (B, C, F) luciferase activity was

765 determined both qualitatively (CCD camera, higher panel) and quantitatively
766 (microplate luminescence reader, lower panel). These experiments were repeated at
767 least 3 times with similar results.
768
769 **Figure 5. RipAC inhibits effector-triggered immunity.**
770 (A-C) RipAC suppresses AtMKK7DD-triggered responses in *N. benthamiana*.
771 RipAC-GFP or the GFP control were transiently expressed in 5-week-old *N.*
772 *benthamiana* leaves 24-hours prior to AtMKK7DD expression. (A) Photograph 5 dpi
773 with Agrobacterium leading to the expression of AtMKK7DD. The number beside the
774 photograph indicates the ratios of infiltration showing cell death suppression to total
775 number of infiltrations. (B) Western blot showing the accumulation of RipAC-GFP,
776 AtMKK7DD-GFP, free GFP, and phosphorylated MAPKs one day after AtMKK7DD
777 expression. (C) Quantification of pMAPK in (B). The intensity of the pMAPK bands in
778 RipAC-GFP expression sample is represented relative to the intensity in the GFP
779 control (mean ± SEM, data from 3 independent biological repeats). (D-G) RipAC
780 suppresses effector-triggered immunity in Arabidopsis. Leaves of WT (WT) and
781 RipAC-transgenic lines (AC #3 and AC #31) were hand-infiltrated with *Pto* empty
782 vector (EV, D), *Pto* AvrRpm1 (E), *Pto* AvrRpt2 (F), or *Pto* AvrRps4 (G). Samples were
783 taken 3dpi (mean ± SEM, n=6, ** $p<0.01$, *t*-test). These experiments were repeated at
784 least 3 times with similar results.
785

786 **Figure 6. MAPK-mediated phosphorylation is important for SGT1 function in the**
787 **activation of ETI.**
788 (A) AtSGT1a and AtSGT1b associate with MAPK4 and MAPK6 in plant cells. CoIPs
789 were performed as in Fig. 4E. (B) MAPK activation triggered by AvrRpt2 expression
790 correlates with increased AtSGT1 phosphorylation at T346. Twelve-day-old
791 Dex:AvrRpt2 plants were treated with 30 mM Dex, and samples were taken at the
792 indicated time points. In (B), a custom antibody was used to detect the
793 phosphorylated peptide containing AtSGT1 T346. (C) Quantitation of pSGT1b signal
794 relative to actin in (B). pSGT1 was normalized to the signal intensity in 0 hpi (mean ±
795 SE of 4 independent biological repeats, ** $p<0.01$, *t*-test). (D) A phospho-mimic
796 mutation in AtSGT1b T346 (T346D) promotes cell death triggered by RPS2
797 overexpression. Agrobacterium expressing AtSGT1b variants or the GUS-FLAG
798 control (OD600=0.5) were infiltrated into *N. benthamiana* leaves 1 day before
799 infiltration with Agrobacterium expressing RPS2 (OD600=0.15). Leaf discs were taken
800 21 hpi for conductivity measurements at the indicated time points. The time points in
801 the x-axis are indicated as hpi with Agrobacterium expressing RPS2 (mean ± SEM,
802 n=4, ** $p<0.01$, *t*-test, 3 replicates). (E, F) Observation of RPS2-triggered cell death by
803 visible light (E) and UV light (F). The Agrobacterium combinations were infiltrated as
804 described in (D), and the cell death phenotype was recorded 4 dpi with Agrobacterium
805 expressing RPS2. (G) Phospho-mimic mutations in AtSGT1b S271 and T346 (DD) do
806 not affect RAR1-SGT1 complex formation. Split-LUC assays were performed as in the
807 Fig. 3D. (H) A phospho-mimic mutation in AtSGT1b T346 (T346D) disrupts

808 RPS2-SGT1b association. Quantitation of the luciferase signal was performed as in
809 the Fig. 4B. The nomenclature of the AtSGT1b mutants used is: 1A=S271A,
810 1D=S271D, 2A=T346A, 2D=T346D, AA=S271AT346A, DD=S271DT346D. The
811 experiments shown in Figure 6 were performed at least 3 times with similar results.
812 See also Figures S6 and S7.
813
814 **Figure 7. RipAC interferes with MAPK-SGT1 interaction to suppress SGT1**
815 **phosphorylation.**
816 (A) RipAC reduces SGT1 phosphorylation in Arabidopsis. SGT1 phosphorylation was
817 determined in twelve-day-old Col-0 WT and RipAC transgenic lines (AC #3 and AC
818 #31) by western blot. Custom antibodies were used to detect the accumulation of
819 SGT1 and the presence of a phosphorylated peptide containing AtSGT1 T346. (B)
820 Quantitation of SGT1 and pSGT1b signal normalized to actin and relative to Col-0 WT
821 samples in (A) (mean ± SEM, n=9, p-values are shown, *t*-test). (C) RipAC suppresses
822 ETI-triggered SGT1 phosphorylation in Arabidopsis protoplasts. Western blots were
823 performed as in (A) using samples from protoplasts 10 hours after transfection with
824 the indicated constructs. (D) Quantitation of pSGT1b signal normalized to actin and
825 relative to the control sample transfected with GUS and GFP in (C) (mean ± SEM of 3
826 independent biological replicates, * $p<0.05$, ** $p<0.01$, *t*-test). (E, F) Competitive
827 Split-LUC assays showing that RipAC interferes with the interaction between MAPK3
828 (E) / MAPK4 (F) and AtSGT1b. In quantitative assays, the graphs show the mean
829 value ± SEM (n=8, ** $p<0.01$, *t*-test). (G) Competitive CoIP showing that RipAC

830 interferes with the interaction between MAPK6 and AtSGT1b. Anti-FLAG beads were
831 used to IP MAPK6. In all the competitive interaction assays, in addition to the
832 interaction pair, RipAC or CBL-GFP (as negative control) were expressed to
833 determine interference. In (E, F) luciferase activity was determined both qualitatively
834 (CCD camera, higher panel) and quantitatively (microplate luminescence reader,
835 lower panel). These experiments were repeated at least 3 times with similar results.

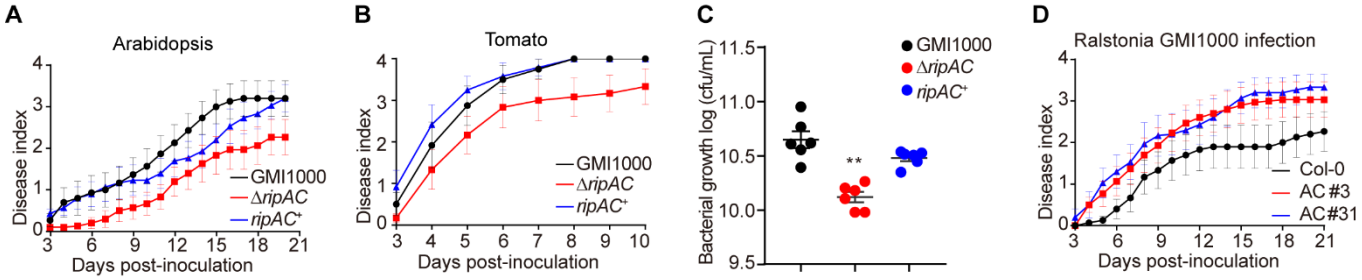

Figure 1. RipAC contributes to *Ralstonia solanacearum* virulence in Arabidopsis and tomato. (A, B) Soil-drenching inoculation assays in Arabidopsis (A) and tomato (B) were performed with GMI1000 WT, Δ*ripAC* mutant, and RipAC complementation (*ripAC*⁺) strains. n=15 plants per genotype (for Arabidopsis) or n=12 plants per genotype (for tomato). The results are represented as disease progression, showing the average wilting symptoms in a scale from 0 to 4 (mean ± SEM). (C) Growth of *R. solanacearum* GMI1000 WT, Δ*ripAC* mutant, and RipAC complementation (*ripAC*⁺) strains in tomato plants. 5 µL of bacterial inoculum (10^6 cfu mL^{-1}) were injected into the stem of 4-week-old tomato plants and xylem sap was taken from each infected plants for bacterial titer calculation 3 days post-inoculation (dpi) (mean ± SEM, n=6, ** $p<0.01$, *t*-test). (D) Soil-drenching inoculation assays in Col-0 WT and RipAC-expressing Arabidopsis lines (AC #3, AC #31, two independent lines) with GMI1000 WT strain. Results are represented as in A and B.
See also Figures S1, S2 and S3.

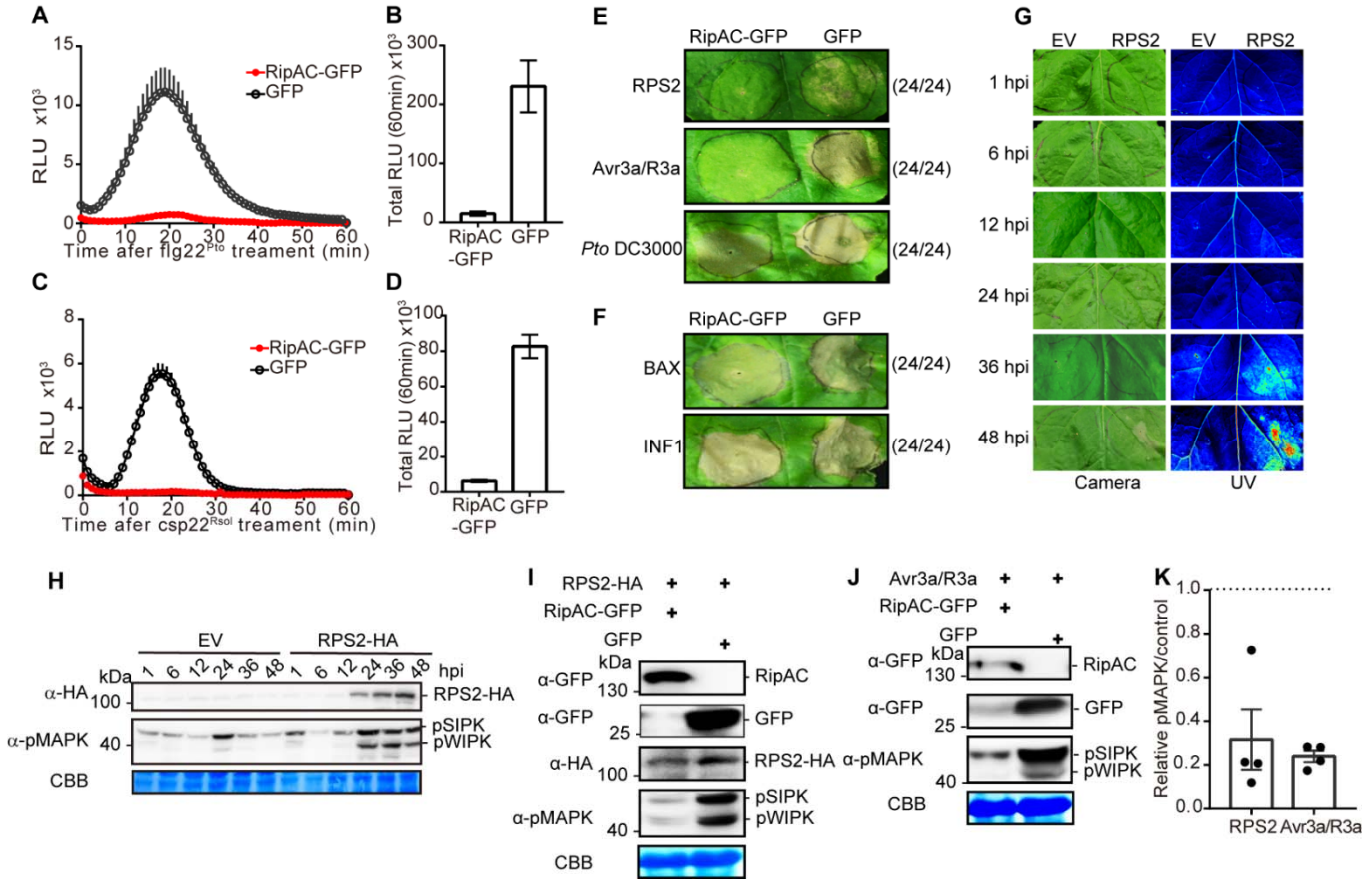

Figure 2. RipAC inhibits plant immune responses in *Nicotiana benthamiana* leaves.
(A-D) RipAC suppresses ROS burst triggered by flg22^{Pto} (A and B) and csp22^{Rsol} (C and D). RipAC-GFP or GFP (as control) were transiently expressed in 5-week-old for flg22) or 6-week-old (for csp22) *N. benthamiana* leaves and ROS burst was analyzed after treatment with the respective elicitors (50 nM) using a luminol-based assay (mean ± SEM, n=24). These experiments were performed at least 3 times with similar results. (E) RipAC suppresses RPS2-, Avr3a/R3a-, *Pto* DC3000-associated cell death. (F) RipAC does not suppress BAX- or INF1-induced cell death. Photographs were taken 5 days after the expression of the cell death inducer. The numbers beside the photographs indicate the ratios of infiltration showing the presented result among the total number of infiltrations. (G and H) Activation of the MAPKs NbSIPK and NbWIPK induced by RPS2. (G) RPS2-triggered cell death was monitored by visible light and UV light. (H) Phosphorylation of NbSIPK and NbWIPK was detected using anti-pMAPK antibody. (I and J) RipAC suppresses MAPK activation triggered by the overexpression of RPS2 (I) or Avr3a/R3a (J). (K) Quantification of relative pMAPK in (I) and (J). The quantification of the pMAPK band in RipAC expression spots is represented relative to the intensity in the GFP control in each assay (mean ± SEM of 4 independent biological replicates).

A

Protein	Peptide sequence	Mascot Ion Score
SGT1	(K)AALETGASLAPAESR(F)	85.6
	(K)AEPLHWTSLEYTR(E)	28.3

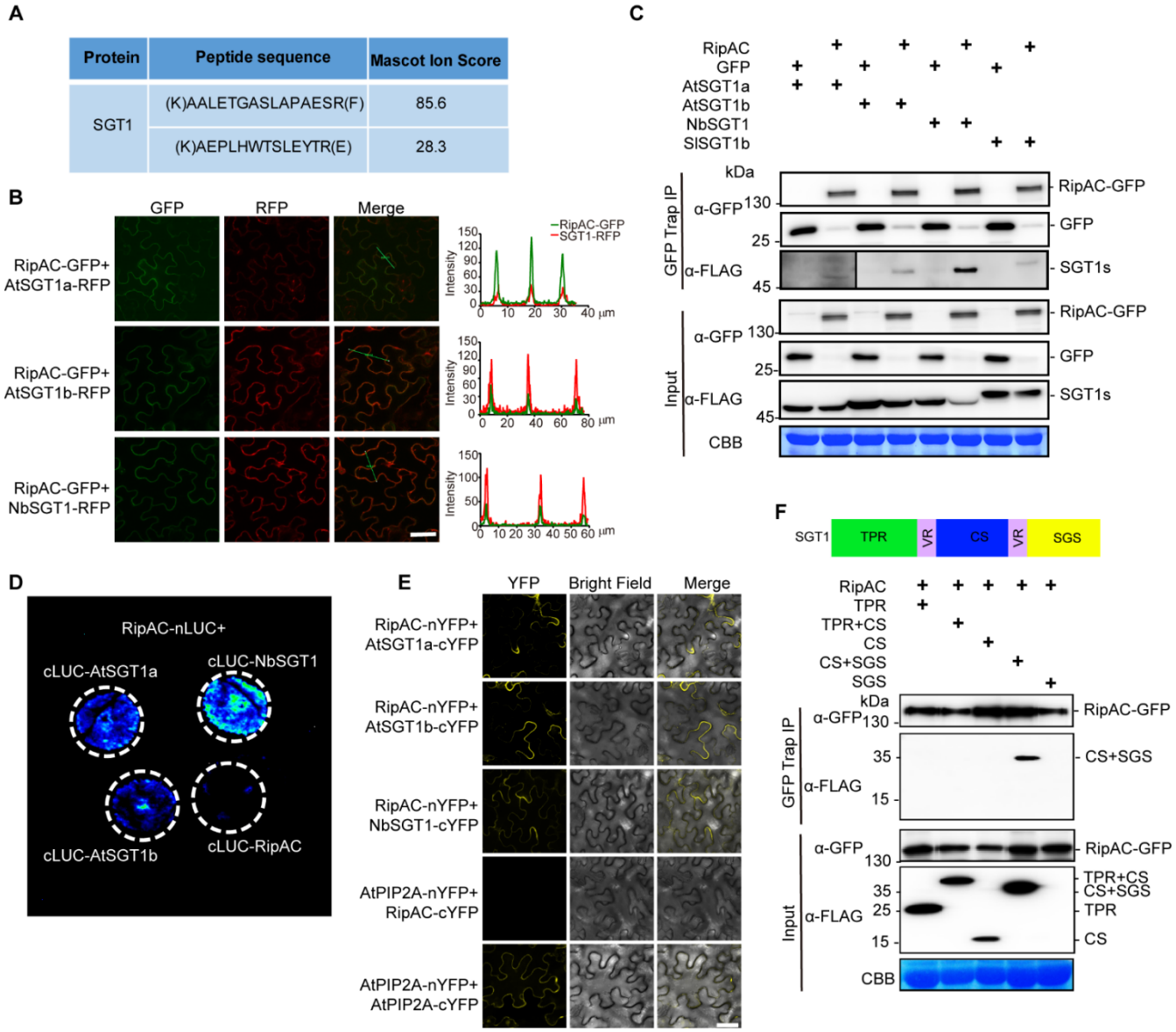

Figure 3. RipAC associates with SGT1 in plant cells.
(A) RipAC-GFP or free GFP were transiently expressed in *N. benthamiana* leaves. The figure shows the unique NbSGT1 peptides identified exclusively in RipAC-GFP sample upon GFP immunoprecipitation followed by IP-MS/MS analysis. (B) RipAC-GFP co-localizes with SGT1-RFP in plant cells. RipAC-GFP was transiently co-expressed with SGT1-RFP (AtSGT1a, AtSGT1b, or NbSGT1), and the GFP fluorescence signal was observed 48 hpi using confocal microscopy. The images show the fluorescence from GFP, RFP channel, and the merged fluorescence from both channels. The corresponding fluorescence intensity profiles (GFP, green; RFP, red) across the green lines are shown. Scale bar=50 μm. (C) CoIP to determine interactions between RipAC and SGT1s. The signal in the interaction between RipAC and AtSGT1a was weak and is shown with longer exposure. (D) Split-LUC assay, and (E) split-YFP complementation assay, to determine direct interaction between RipAC and SGT1 in plant cells. In (E), the self-association of aquaporin AtPIP2A was used as a positive interaction control, while the RipAC-AtPIP2A combination was used as a negative control. Scale bar=50 μm. (F) CoIP to determine interactions between RipAC and different truncated versions of NbSGT1. The diagram summarizes the different domains of SGT1: TPR, N-terminal tetratricopeptide repeat (TPR) domain; CS, CHORD-SGT1 domain; SGS, C-terminal SGT1-specific domain; VR, variable region. In C-F, each combination of proteins shown was transiently expressed in *N. benthamiana* and samples were taken 2 dpi. Experiments shown in (B-E), were performed 3 times with similar results. The experiment shown in (F) was performed twice.
See also Figure S4.

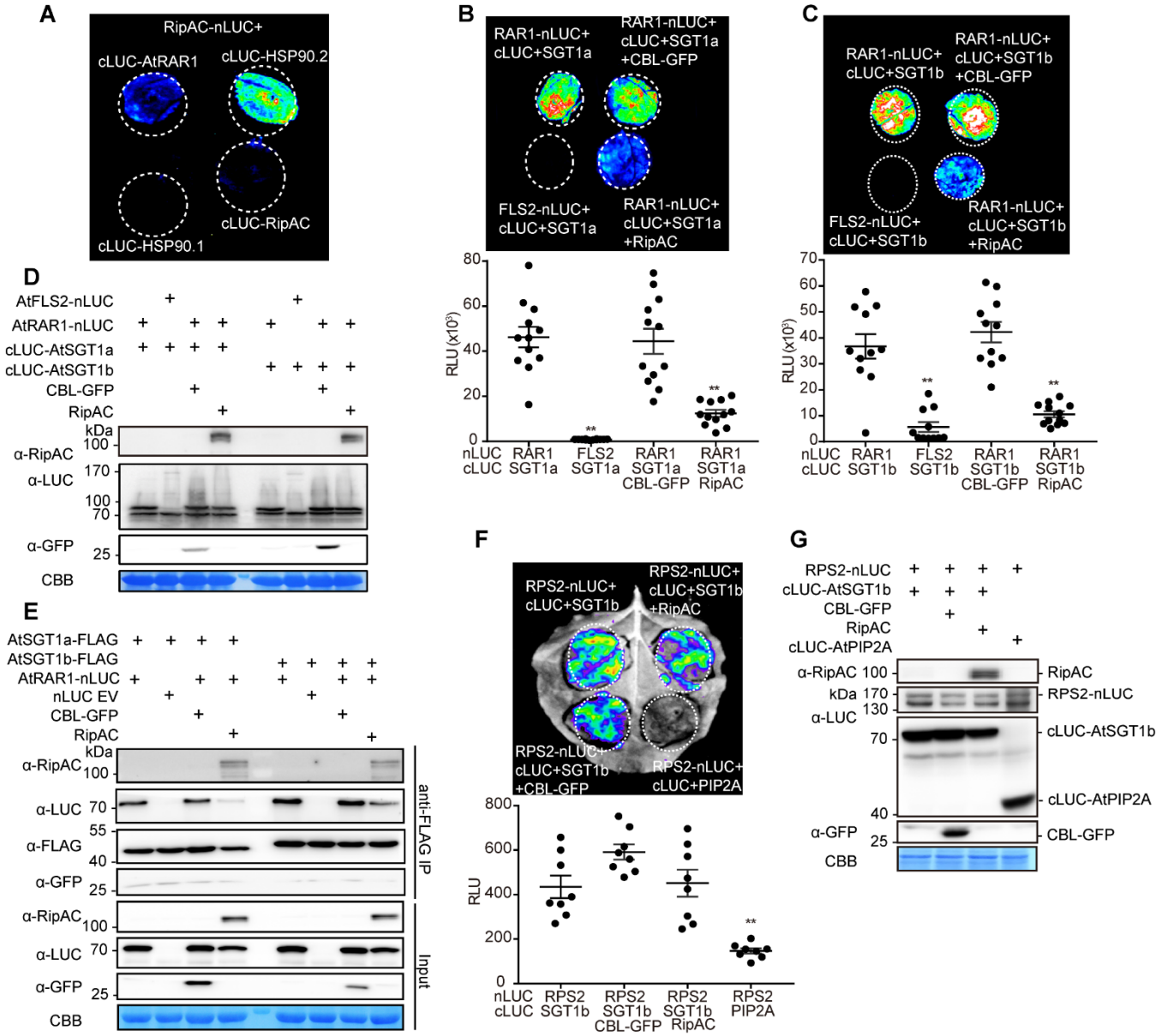

Figure 4. RipAC interferes with the SGT1-RAR1 complex.
(A) RipAC associates with SGT1, RAR1, and HSP90. Split-LUC assay was performed as in the Fig. 3D. (B) and (C) Competitive Split-LUC assays showing that RipAC interferes with SGT1a/b-RAR1 complex formation. The FLS2-SGT1 combination was used as negative interaction control. In quantitative assays, the graphs show the mean value ± SEM (n=12, ** p<0.01, *t*-test). (D) Protein accumulation from (B) and (C). (E) Competitive CoIP showing that RipAC interferes with SGT1a/b-RAR1 complex formation. Anti-FLAG beads were used to IP AtSGT1a and AtSGT1b. (F) Competitive Split-LUC showing that RipAC does not interfere with RPS2-SGT1b association. (G) Western blot shows the protein accumulation in (F). The RPS2-PIP2A combination was used as negative control. In all the competitive interaction assays, in addition to the interaction pair, RipAC or CBL-GFP (as negative control) were expressed to determine interference. In (B, C, F) luciferase activity was determined both qualitatively (CCD camera, higher panel) and quantitatively (microplate luminescence reader, lower panel). These experiments were repeated at least 3 times with similar results.

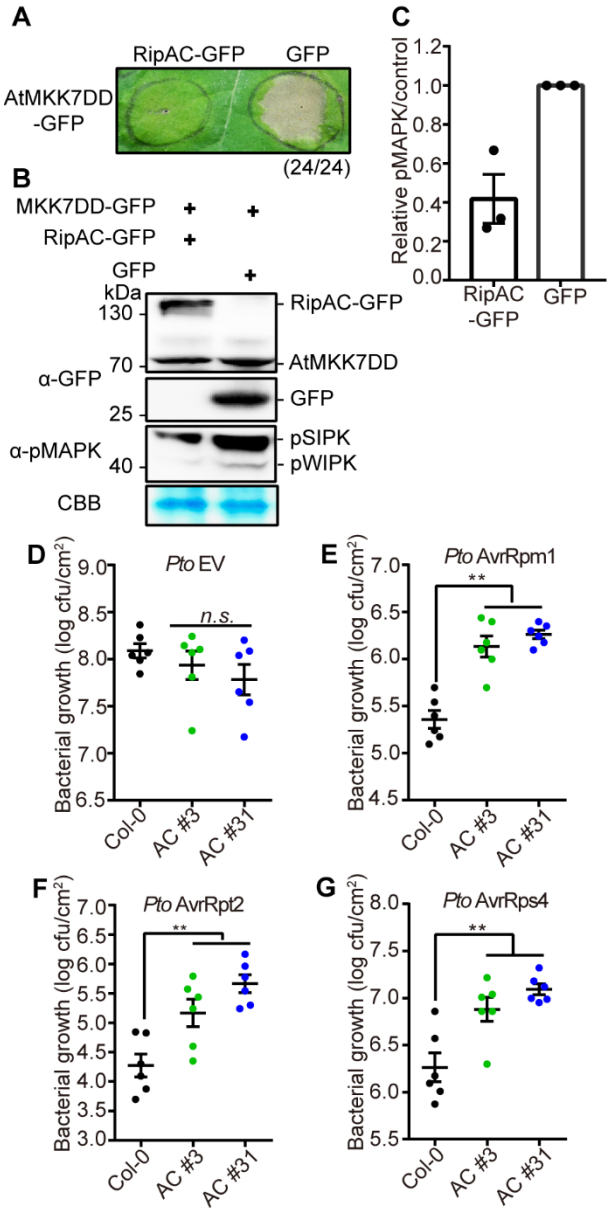

Figure 5. RipAC inhibits effector-triggered immunity.
(A-C) RipAC suppresses AtMKK7DD-triggered responses in *N. benthamiana*. RipAC-GFP or the GFP control were transiently expressed in 5-week-old *N. benthamiana* leaves 24-hours prior to AtMKK7DD expression. (A) Photograph 5 dpi with Agrobacterium expressing AtMKK7DD. The number beside the photograph indicates the ratios of infiltration showing cell death suppression to total number of infiltrations. (B) Western blot showing the accumulation of RipAC-GFP, AtMKK7DD-GFP, free GFP, and phosphorylated MAPKs one day after AtMKK7DD expression. (C) Quantification of pMAPK in (B). The intensity of the pMAPK bands in RipAC-GFP expression sample is represented relative to the intensity in the GFP control (mean ± SEM, data from 3 independent biological repeats). (D-G) RipAC suppresses effector-triggered immunity in Arabidopsis. Leaves of WT (WT) and RipAC-transgenic lines (AC #3 and AC #31) were hand-infiltrated with *Pto* empty vector (EV, D), *Pto* AvrRpm1 (E), *Pto* AvrRpt2 (F), or *Pto* AvrRps4 (G). Samples were taken 3dpi (mean ± SEM, n=6, ** $p<0.01$, *t*-test). These experiments were repeated at least 3 times with similar results.

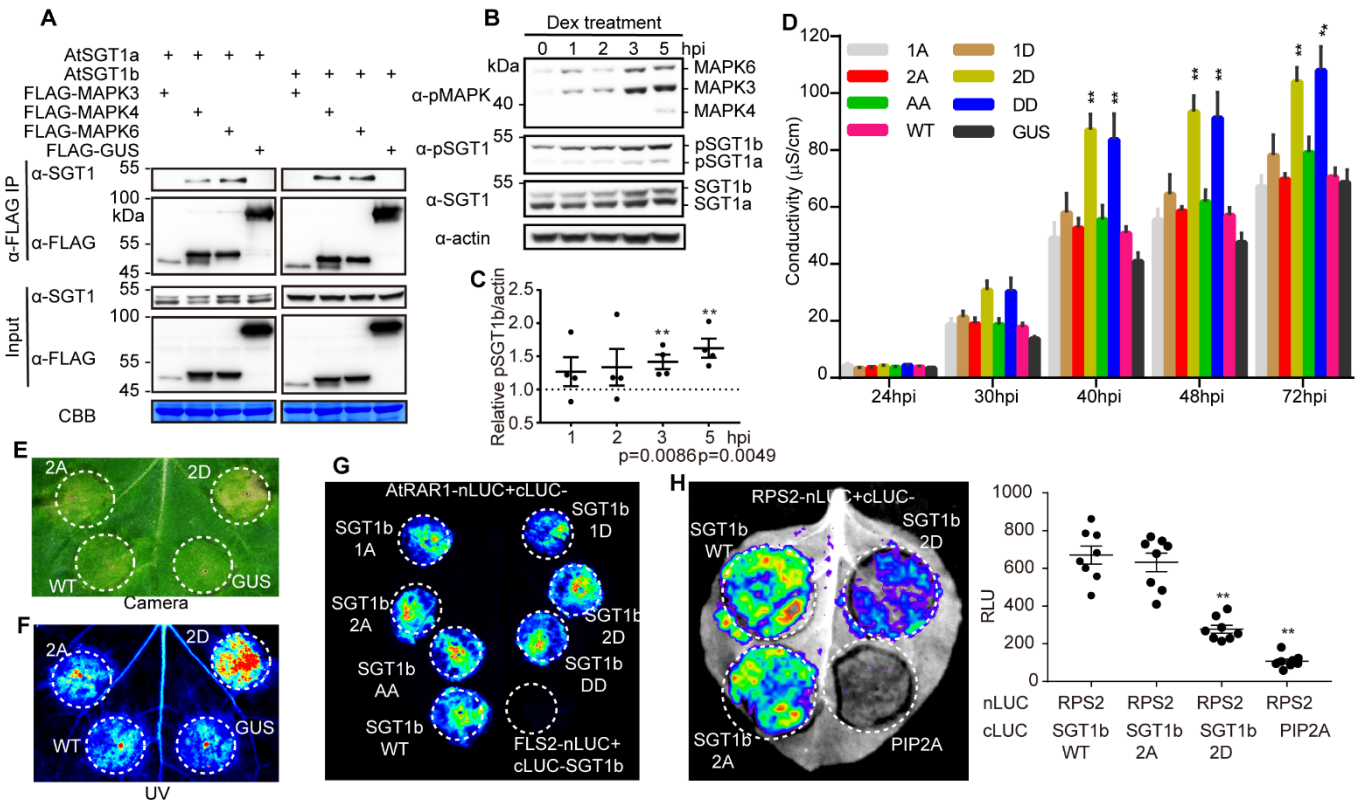

Figure 6. MAPK-mediated phosphorylation is important for SGT1 function in the activation of ETI.
(A) AtSGT1a and AtSGT1b associate with MAPK4 and MAPK6 in plant cells. CoIPs were performed as in Fig. 4E. (B) MAPK activation triggered by AvrRpt2 expression correlates with increased AtSGT1 phosphorylation at T346. Twelve-day-old Dex:AvrRpt2 plants were treated with 30 μM Dex, and samples were taken at the indicated time points. In (B), a custom antibody was used to detect the phosphorylated peptide containing AtSGT1 T346. (C) Quantitation of pSGT1b signal relative to actin in (B). pSGT1 was normalized to the signal intensity in 0 hpi (mean ± SE of 4 independent biological repeats, ** p<0.01, *t*-test). (D) A phospho-mimic mutation in AtSGT1b T346 (T346D) promotes cell death triggered by RPS2 overexpression. Agrobacterium expressing AtSGT1b variants or the GUS-FLAG control (OD600=0.5) were infiltrated into *N. benthamiana* leaves 1 day before infiltration with Agrobacterium expressing RPS2 (OD600=0.15). Leaf discs were taken 21 hpi for conductivity measurements at the indicated time points. The time points in the x-axis are indicated as hpi with Agrobacterium expressing RPS2 (mean ± SEM, n=4, ** p<0.01, *t*-test, 3 replicates). (E, F) Observation of RPS2-triggered cell death by visible light (E) and UV light (F). The Agrobacterium combinations were infiltrated as described in (D), and the cell death phenotype was recorded 4 dpi with Agrobacterium expressing RPS2. (G) Phospho-mimic mutations in AtSGT1b S271 and T346 (DD) do not affect RAR1-SGT1 complex formation. Split-LUC assays were performed as in the Fig. 3D. (H) A phospho-mimic mutation in AtSGT1b T346 (T346D) disrupts RPS2-SGT1b association. Quantitation of the luciferase signal was performed as in the Fig. 4B. The nomenclature of the AtSGT1b mutants used is: 1A=S271A, 1D=S271D, 2A=T346A, 2D=T346D, AA=S271AT346A, DD=S271DT346D. The experiments shown in Figure 6 were performed at least 3 times with similar results.
See also Figures S6 and S7.

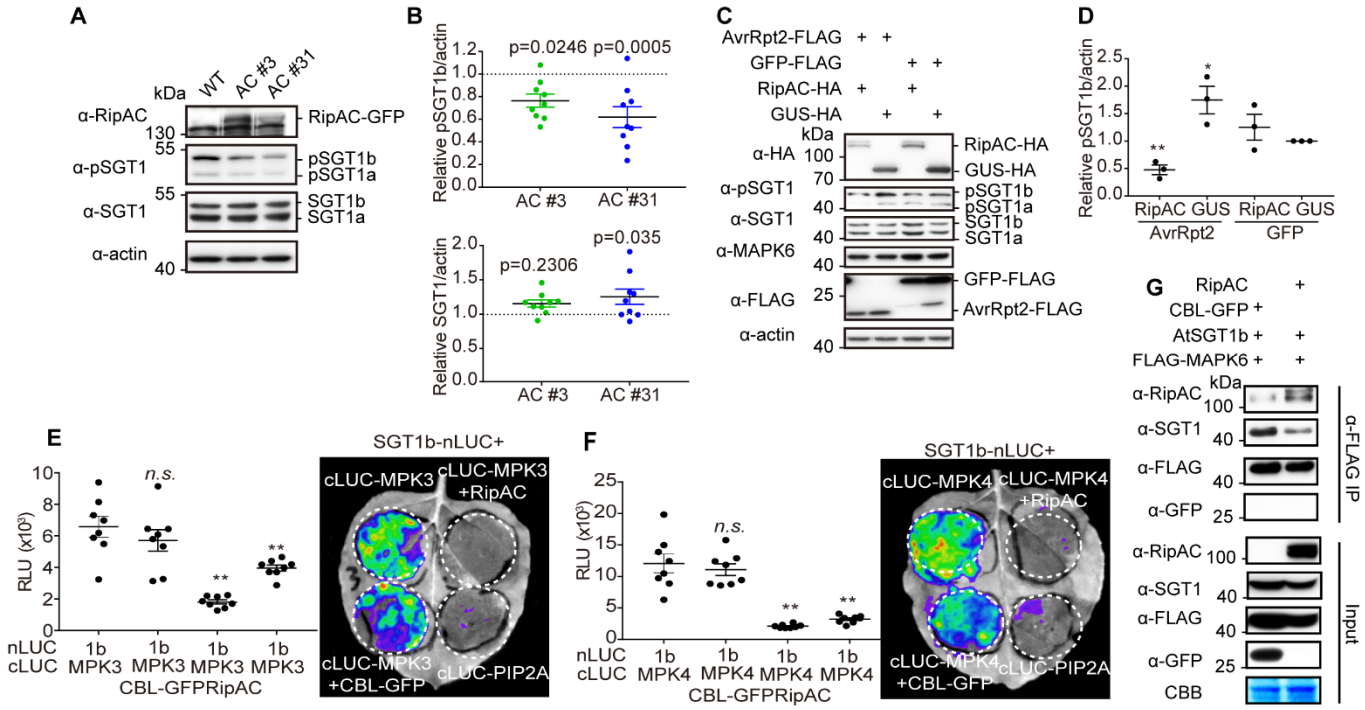

Figure 7. RipAC interferes with MAPK-SGT1 interaction to suppress SGT1 phosphorylation.
(A) RipAC reduces SGT1 phosphorylation in Arabidopsis. SGT1 phosphorylation was determined in twelve-day-old Col-0 WT and RipAC transgenic lines (AC #3 and AC #31) by western blot. Custom antibodies were used to detect the accumulation of SGT1 and the presence of a phosphorylated peptide containing AtSGT1 T346. (B) Quantitation of SGT1 and pSGT1b signal normalized to actin and relative to Col-0 WT samples in (A) (mean ± SEM, n=9, p-values are shown, *t*-test). (C) RipAC suppresses ETI-triggered SGT1 phosphorylation in Arabidopsis protoplasts. Western blots were performed as in (A) using samples from protoplasts 10 hours after transfection with the indicated constructs. (D) Quantitation of pSGT1b signal normalized to actin and relative to the control sample transfected with GUS and GFP in (C) (mean ± SEM of 3 independent biological replicates, * $p<0.05$, ** $p<0.01$, Student's *t*-test). (E, F) Competitive Split-LUC assays showing that RipAC interferes with the interaction between MAPK3 (E) / MAPK4 (F) and AtSGT1b. In quantitative assays, the graphs show the mean value ± SEM (n=8, ** $p<0.01$, *t*-test). (G) Competitive CoIP showing that RipAC interferes with the interaction between MAPK6 and AtSGT1b. Anti-FLAG beads were used to IP MAPK6. In all the competitive interaction assays, in addition to the interaction pair, RipAC or CBL-GFP (as negative control) were expressed to determine interference. In (E, F) luciferase activity was determined both qualitatively (CCD camera, higher panel) and quantitatively (microplate luminescence reader, lower panel). These experiments were repeated at least 3 times with similar results.